Pergamon

Int. J. Solids Structures Vol. 31, No. 18, pp. 2477–2490, 1994

0020–7683/94 $7.00 + .00

0020-7683(94)E0036-U

PLASTIC DEFORMATION ANALYSIS OF CRACKED ADHESIVE BONDS LOADED IN SHEAR

MARTIN Y. M. CHIANG
Polymers Division, National Institute of Standards and Technology, Gaithersburg, MD 20899, U.S.A.

and

HERZL CHAI
Department of Mechanics, Materials and Structures, School of Engineering, Tel Aviv University, Tel Aviv, Israel

(*Received* 7 *October* 1993; *in revised form* 2 *March* 1994)

Abstract—The plane strain elastoplastic stress field around an interface crack in adhesively bonded joints deforming in shear was determined from a large strain, incremental plasticity finite element analysis. Two particular specimens were analysed, i.e. the end-notched flexure and the end-loaded split, with the bond thickness varying from 18 μm to 0.4 mm. The yield behavior of the adhesive was modeled by the von Mises (J_2) and the extended Drucker–Prager (EDP) material models, the latter being more appropriate to polymeric adhesives. Associated and non-associated flow rules were considered for the J_2 and EDP models, respectively. The adhesive stress–strain response was assumed to be elastoplastic, and it incorporated various levels of strain hardening. The analysis shows that the stresses at the crack tip are triaxial, with the deformations dominated by the shearing component, the latter being localized at the very edge of the crack tip, an effect which tended to increase with increasing bond thickness or decreasing degree of strain hardening. The numerical predictions of the length of the plastic zone that developed ahead of the crack tip and of the distribution of average shear strain across the bond within that zone agreed well with experimental results. In contrast with the behavior for the analogous mode I loading case, the mean stress declined monotonically with increasing distance from the crack tip.

1. INTRODUCTION

The mechanical performance of a glue binding two distinct material phases is of interest in a variety of industrial and technological applications, including traditional adhesive bonding, composite materials, microlamination and electronic packaging. Fracture mechanics is a concept which has been widely used for assessing bond strength, but the majority of theoretical treatments are limited to linearly elastic adhesive behavior (Trantina, 1972; Anderson *et al.*, 1977; Wang and Yau, 1982; Hutchinson and Suo, 1991; Akisanya and Fleck, 1992). For tough adhesive systems, however, considerably long plastic deformation zones (i.e. more than two orders of magnitude greater than the bond thickness) may develop ahead of the crack tip prior to crack propagation (Hunston *et al.*, 1989; Liechti and Freda, 1989; Chai, 1992). In fact, even brittle adhesives display a ductile stress–strain response when the bond thickness is decreased to a few micrometers (Chai, 1993b). For such applications, use of linear elastic fracture mechanics (LEFM) is clearly inappropriate.

Most treatments of interlayer nonlinearity in bonded joints are variations of the shear-lag concept (Tirosh, 1973; Hart-Smith, 1981; Chatterjee, 1991; Chai, 1992; Suo *et al.*, 1992), which is based on several simplifications including stress uniformity across the bond, neglect of all interlayer stresses but the shear stress and an elastic–perfectly plastic adhesive behavior. While this concept may be useful for predicting global mechanical responses (i.e. specimen deflection, plastic zone length, etc.) in slender structural components, it is inadequate for elucidating the local behavior at the crack tip, where the material actually fails. Rigorous plasticity analyses of cracked adhesive bonds are scarce. The most exhaustive treatment seems to be due to Varias *et al.* (1991), who employed the finite element technique in conjunction with incremental plasticity and a J_2 material model to study the stress

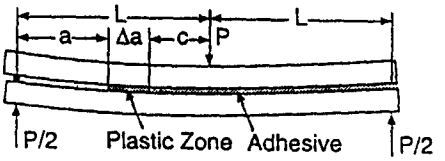

(a) End-Notched Flexure (ENF)

L=101.6 mm, a=50.8 mm, h=9.5 mm

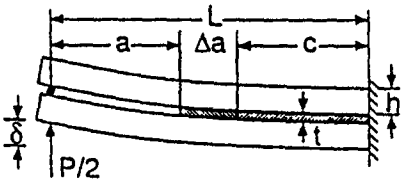

(b) End-Loaded Split (ELS)

Fig. 1. ENF and ELS adhesive bonding specimens.

distribution in the plastic zone at the crack tip in a constrained metal foil subjected to a remote mode I loading. The finite element technique was also used to evaluate the elastoplastic stresses in a layered structure containing a crack lying perpendicularly to the lamination plane (Cao and Evans, 1991).

In this work, the finite element code ABAQUS (1992) was employed to obtain the large strain elastoplastic stress state in the adhesive for the end-notched flexure (ENF) and end-loaded split (ELS) specimens shown in Fig. 1. These specimens are commonly used for evaluating the mode II fracture toughness of laminated composites and adhesively bonded joints. In addition, their relative simplicity provides insight to the understanding of fracture in more complex adhesive bonding configurations. Experiments show that the adhesive thickness, t, plays a major role on the fracture conditions in the bond (Chai, 1988). Therefore, t was set as a variable in this study, ranging from 18 μm to 0.4 mm. Global quantities such as plastic zone length and across-the-bond average shear strain along that zone are compared with experimental data (Chai, 1988) as well as with a previously developed shear-lag analysis (Chai, 1992). The applicable range of the shear-lag model is assessed from comparison with finite element results for various slenderness ratios of the split beam. In addition, some general observations concerning the local behavior at the crack tip are made; a more exhaustive investigation of this is deferred to future work.

The majority of elastoplastic stress analyses of adhesively bonded joints treat the adhesive interlayer in accordance with the J_2 yield criterion (Tirosh, 1973; Chatterjee, 1991; Varias *et al.*, 1991; Cao and Evans, 1991; Chai, 1992; Suo *et al.*, 1992). However, it is well known that for polymeric adhesives, which are of particular interest in this work, the yield conditions depend on pressure and follow closely a modified Mohr–Coulomb yield criterion (Argon *et al.*, 1968; Bauwens, 1970; Brady and Yeh, 1971; Bowden and Jukes, 1972). For this reason, the latter type of material model was also included in this study.

2. NUMERICAL ANALYSIS

The finite element program was employed to study the specimens shown in Fig. 1. The plane strain and the large strain options were invoked. The width of the specimens was 25.4 mm. Consistent with experimental observations (Chai, 1993a), the crack was assumed to lie along one of the two metal/matrix interfaces. The adherends were assumed linearly elastic while the interlayer was elastoplastic.

2.1. *Materials and geometry*

The materials, geometry and loading conditions for the specimens in Fig. 1 were chosen to simulate the fracture experiments (Chai, 1988, 1992, 1993a). In this figure, a and Δa

Table 1. Material properties

Material	E (GPa)	ν	γ_y	τ_0 (MPa)	G_{IC} (N/M)
Adherends (aluminum)	69	0.3			
Adhesive (BP-907)	3.4	0.35	0.06	75	500

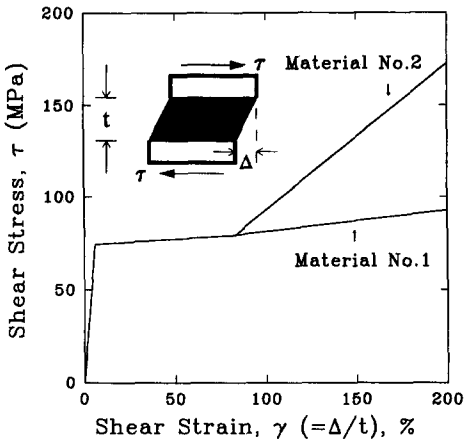

Fig. 2. The stress–strain responses of two elastoplastic adhesive used in the finite element analysis. Also shown is a model specimen for producing a state of simple shear in the adhesive.

denote the crack length and plastic zone length ahead of the crack tip, respectively, while h and L denote the specimen's height and the specimen's span [Fig. 1(b)] or half-span [Fig. 1(a)], respectively. Table 1 lists some material properties used in the finite element analysis. The adherends were 7075 Al alloy, while the adhesive was a toughened epoxy (BP-907†, American Cyanamid Co.). Tests under simple shear conditions using the napkin ring specimen (Chai, 1993b) showed that the stress–strain behavior of this adhesive greatly depends on bond thickness, an effect which may be attributed to a complex interaction of the surfaces of the adherends with voids or microcracks and to material orientation that may develop at large strains. The initial adhesive response was fairly well characterized by an elastic–perfectly plastic behavior, with the yield stress, τ_0, being independent of t. This was followed by a phase of strain hardening which occurred once the engineering shear strain, γ, exceeded 0.83, irrespective of bond thickness. The degree of strain hardening varied with t, however, being nearly zero for $t > 40$ μm while increasing monotonically with decreasing t from 40 μm. The range of material behavior discussed above is simulated in this work by the two curves (i.e. materials 1 and 2) shown in Fig. 2. It is assumed that the unloading path is parallel to the first stress–strain segment in Fig. 2.

The material response is input in ABAQUS (1992) through σ_t vs ε_t, the true stress and true strain, respectively, in a uniaxial tension test, where

$$\varepsilon_t \equiv \ln(1+\varepsilon_E) \tag{1}$$

and ε_E is the engineering strain. The experimental stress–strain data, which are simulated in Fig. 2, are given in the form of shear stress (τ) vs the engineering shear strain (γ). To convert these data into tensile stress vs tensile strain, ABAQUS (1992) was run on the model shear specimen shown in the insert in Fig. 2; this plane strain specimen reproduces the conditions prevalent in the napkin ring shear test. Specifically, a trial relationship for ε_t vs σ_t was input, and the ABAQUS prediction for the engineering shear strain was compared

† Certain commercial materials and software are identified in this paper in order to specify adequately the experimental procedure. In no case does such identification imply recommendation or endorsement by the National Institute of Standards and Technology (NIST) nor does it imply necessarily the best available for the purpose.

with the desired model curve in Fig. 2. The initial guess was subsequently amended and re-run until the desired τ vs γ relationship was reasonably well reproduced. This procedure was repeated for each of the material models employed.

2.2. *Material models*

Referring to Fig. A1 for notations, the Mohr–Coulomb yield criterion is given by Chen and Han (1988)

$$|\tau| = c - \sigma \tan \phi, \tag{2}$$

where τ and σ are the limiting shear stress in the yielding plane and the normal stress on that plane, respectively, and the material constants c and ϕ are the cohesion and angle of internal friction, respectively. It has been shown (Argon *et al.*, 1968; Bauwens, 1970; Brady and Yeh, 1971; Bowden and Jukes, 1972) that eqn 2 describes fairly well the yield behavior of polymeric materials under general loading if the normal stress σ is replaced by the hydrostatic stress.

ABAQUS (1992) offers the extended Drucker–Prager (EDP) material model which, by proper selection of material constants, can be made to simulate well the modified Mohr–Coulomb yield criterion. The yield condition for the EDP model in ABAQUS is

$$\frac{q}{2}\left[1 + \frac{1}{K} - \left(1 - \frac{1}{K}\right)\left(\frac{r}{q}\right)^3\right] + \frac{1}{3}(\sigma_1 + \sigma_2 + \sigma_3)\tan\beta - \left(1 - \frac{1}{3}\tan\beta\right)\sigma_c^0 = 0, \tag{3}$$

where

$$q \equiv \sqrt{3J_2} \tag{4}$$

$$r^3 \equiv \frac{27}{2}J_3 \tag{5}$$

and σ_1, σ_2, σ_3 are the principal stresses, J_2 and J_3 are the second and third invariant of the deviatoric stress tensor, respectively, σ_c^0 is the yield stress in a uniaxial compression test and β and K are material parameters. Defining

$$\lambda \equiv \sigma_c^0/\sigma_t^0, \tag{6}$$

where σ_t^0 is the yield stress in a uniaxial tension test, one can show (see Appendix A) that K and β are related to λ through

$$K = \frac{(\lambda+2)}{(2\lambda+1)} \tag{7}$$

$$\tan\beta = \frac{3(\lambda-1)}{(\lambda+2)}. \tag{8}$$

To completely describe the EDP model, one needs to specify, in addition to σ_c^0 and λ, the parameter ψ, which is the angle between the normal to the yield surface and the increment of plastic strain vector, $d\boldsymbol{\varepsilon}^p$ (ABAQUS, 1992). Associated flow rule is achieved by setting $\psi = \beta$ while $\psi \neq \beta$ corresponds to a non-associated flow. For $\psi = 0$, the material is non-dilatational (no volume change in the plastic deformation regime).

Unfortunately, neither λ nor ψ are known for the BP-907 adhesive considered here. Experiments on a variety of polymeric systems (Bauwens, 1970; Pae and Bhateja, 1971) show that λ typically varies in the range 1.2–1.5. In this study, a value of 1.4 was assumed for λ. In an attempt to select a reasonable value for ψ, a parametric study on the effect of

ψ on the change of volume in the adhesive was performed on the model shear specimen depicted in Fig. 2. The applied shearing displacement was such as to produce 100% shear strain in the deformed adhesive; this value is representative of the ultimate shear strain of the unflawed adhesive when tested as an adhesive bond over the bond thickness range considered in this study (Chai, 1993b). The plastic volume change in the interlayer was found to increase monotonically with ψ, e.g. from 0 to over 100% upon increasing ψ from 0 to 19.44°. The latter choice corresponds to an associated flow if λ is equal to 1.4. Experiments show that polymers suffer only minor volume changes in the yielding or post-yielding deformation regimes (Pampillo and Davis, 1971; Wang *et al.*, 1982). For this reason, ψ was set as zero in the EDP model.

In addition to the EDP model, results were also obtained using the J_2 model which is applicable to metal adhesives. The yield condition in this case is given by (Chen and Han, 1988)

$$\sqrt{J_2} = \tau_0, \tag{9}$$

where τ_0 is the yield stress in a simple shear test. For both the J_2 and the EDP models, isotropic strain hardening was assumed. Such a choice is generally considered to be suitable for problems involving large strains (Rice, 1975). It is noted that large strains may induce anisotropy in polymeric materials, in which case the above assumption may not be strictly correct. Unfortunately, experimental evidence on the post yield behavior of polymers subjected to general loading is scarce.

2.3. *Rate effects*

The finite element results show that large strain gradients tend to develop in the immediate vicinity of the crack tip. This localization effect was found to evolve rapidly during particular segments of the loading, causing instability of the solution process. A common procedure for overcoming such difficulty is to employ dynamic relaxation [e.g. Silling (1988)] which takes into consideration rate dependency of material properties. This tends to slow down rapid changes in the redistribution of field quantities during loading while producing essentially quasi-static stress solutions if sufficient relaxation time is allowed. In ABAQUS, the rate dependency is defined by

$$\dot{\varepsilon}^{\mathrm{pl}} = D(\sigma/\sigma^0 - 1)^d, \tag{10}$$

where $\dot{\varepsilon}^{\mathrm{pl}}$ is the time derivative of the equivalent plastic strain rate, σ is the equivalent stress, σ^0 is the equivalent static yield stress, and D and d are material parameters. Numerical instabilities were encountered in this work only for the EDP material model. In this case, the rate effect [eqn (10)] was invoked, with both D and d taken as unity. Such a choice produced essentially a quasi-static solution while eliminating the numerical instability.

To simulate the experiments (Chai, 1988, 1992, 1993a), the specimens were loaded by a concentrated force P which was incremented up to the critical load for crack propagation over a period of 10 minutes. The specific load increments were independently selected by the numerical routine.

2.4. *Friction*

The effect of adhesive–substrate contact that may develop in the cracked portion of the bond was studied using a built-in contact element in ABAQUS. Interfacial contact was found to be limited to the area of the supporting point and a small region (i.e. on the order of bond thickness) just behind the crack tip. As for a Coulomb type friction, the frictional shear stress, τ_{f}, was assumed proportional to the normal stress, σ_{n}:

$$\tau_{\mathrm{f}} = \alpha\sigma_{\mathrm{n}}, \tag{11}$$

where α is a friction coefficient whose value for certain polymer–metal interfaces is in the range

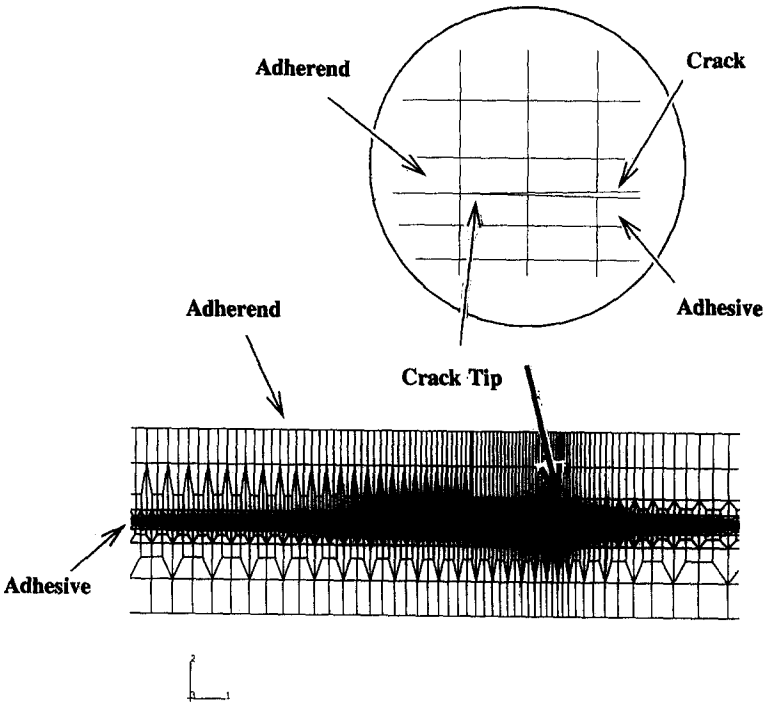

Fig. 3. Finite element mesh at the crack tip vicinity, $t = 18$ μm. The crack lies along the upper adhesive–substrate interface.

0.1–0.3 (Briscoe and Tabor, 1978). A parametric study carried out in this work, where α was varied from 0 to 1, showed that friction has only a marginal effect on all data to be reported in this work.

2.5. *Mesh and convergence*

Four-node isoparametric elements were used to model the adhesive bond specimens, with the element dimensions continuously decreasing towards the crack tip. Figure 3 shows a typical mesh pattern in the crack tip vicinity. At the tip, the mesh is composed of rectangular-grid elements, the vertical dimension of which was typically a bit less than a tenth of the bond thickness. Attempts to further refine the mesh were unsuccessful because of numerical instability of the finite element solution. In contrast to commonly used procedures (Silling, 1988; Varias *et al.*, 1991; Cao and Evans, 1991), no artificial blunting of the crack tip was made. This was because of our desire to correctly model the experimental conditions (Chai, 1993a) and also to gain information on the local behavior of the tip. Convergence of the finite element solution, particularly the strain distribution around the crack tip, was assessed by employing less refined meshes. It was concluded from this study that good convergence of local strain is achieved starting from approximately two to three elements or a quarter bond thickness away from the crack tip.

3. RESULTS

Figures 4(a) and (b) show, respectively, part of the deformed grid for the thickest (0.4 mm) and thinnest (18 μm) bonds studied. The adhesive stress–strain relations used for these cases approximate those obtained from shear tests on the unflawed adhesive at corresponding bond thicknesses (Chai, 1993b). The load P for each case corresponds to the critical load for crack propagation as found in the fracture experiments (Chai, 1988, 1992, 1993a). The results pertain to the EDP model, with $\lambda = 1.4$ and $\psi = 0$. Figure 4(a) shows that the adhesive deforms mostly in shear, with particularly large shear strain at the immediate crack tip vicinity. The magnitude of this local shear strain is several times the average shear strain, $\bar{\gamma}$ (i.e. the relative shear displacement across the bond, Δ, divided by

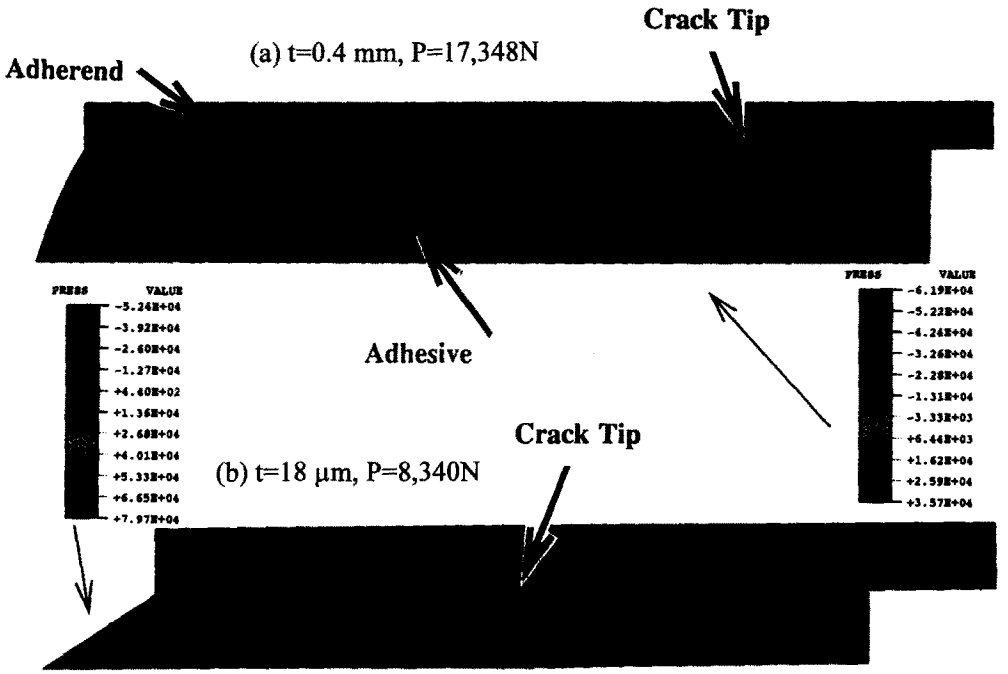

Fig. 4. The deformed grid and contours of $-3\sigma_m$ (in units of 6.8948×10^3 Pa) at the crack tip vicinity, where $\sigma_m = (\sigma_1+\sigma_2+\sigma_3)/3$ is the mean stress. ENF specimen, EDP material model with $\lambda = 1.4$ and $\psi = 0$. The applied loads in (a) and (b) correspond to experimentally obtained critical loads for crack propagation for these bond configurations (Chai, 1988). Shown in each case is part of the upper adherend and the entire adhesive thickness.

t) at the crack tip. Several bond thicknesses ahead of the crack tip, however, the shear strain becomes homogeneous. It is interesting to note that, while in the bondline direction, the plastic strain persists up to a distance of 21 mm, in the thickness direction near the crack tip. The plastic strain occupies only part of the bond; in the rest of the thickness the strains remain elastic. Another observation from Fig. 4(a) is that contact between the adhesive and the substrate is limited to a region about three grids long (much less than one bond thickness) immediately behind the crack tip. The results for the thin adhesive interlayer [Fig. 4(b)] differ from those of the thick bond primarily by the less pronounced strain localization. The shear strain in this case is plastic throughout the thickness of the bond, and it becomes completely homogeneous after a distance of approximately one bond thickness ahead of the tip. One observes that adhesive–substrate contact now persists over a distance of several bond thicknesses behind the tip. Also, although the load in Fig. 4(a) greatly exceeds that of Fig. 4(b), the critical average shear strain for the thick bond is much less than that for the thin bond (i.e. 0.6 vs 1.8). At the very edge of the tip, the first few elements in Figs 4(a) and (b) seem uncharacteristically distorted, which raises concern about the data precision in that region. Indeed, a convergence study using different mesh sizes showed that the adhesive shear strain converged satisfactorily only outside these elements.

Figures 5(a) and (b) show the finite element prediction of the variations with load of the plastic zone length Δa and of $\bar{\gamma}$ at the tip for 18 μm and 0.4 mm thick bonds. Also shown [Figs 5(c, d)] are the distributions of $\bar{\gamma}$ ahead of the crack tip for a given load and the variations of the load-point deflection, δ, with load. The loads in Fig. 5(c) correspond to the fracture loads as obtained in experiments pertaining to the same bond configurations (Chai, 1988, 1992, 1993a). Results are given for the EDP and the J_2 material models. All the data in these figures were produced using the ENF specimen. Selected data generated using the ELS specimen showed that the difference in the results between these two specimens was marginal. As shown in Figs 5(a–d), the difference between the predictions of the EDP and J_2 models is negligible. Figure 5(a) shows that a measurable plastic zone develops once P is increased from a certain value, which depends on t, and that the critical length of the plastic zone is overwhelmingly greater than the bond thickness. The average shear strain increases rapidly toward the crack tip [Fig. 5(c)], reaching, in the case of the 18 μm thick bond, a value as large as 180%.

Figure 6 (solid curve) shows the variations of the critical length of the plastic zone, Δa_{cr} (i.e. the length of the plastic zone ahead of the crack tip at the time of crack propagation) with bond thickness. This curve is a fit to numerical results pertaining to the seven bond thicknesses listed in the figure. The corresponding loads and material choices are also listed in the figure, respectively. The loads are the critical loads obtained from the fracture experiments (Chai, 1988, 1992) and the material choices are the simulation of stress–strain curves (Fig. 2) obtained in the napkin ring tests (Chai, 1993b). As shown, Δa_{cr} is quite fixed for $t > 0.15$ mm while declining monotonically for thinner bonds. Its value in the micrometer thickness range is several millimeters.

4. COMPARISON WITH EXPERIMENTS

Figures 5(a,b,d) and 6 show experimental data pertaining to variations with load P of Δa, $\bar{\gamma}$ at the crack tip and δ, and the variations of Δa_{cr} with t, in that order. These data were obtained from analysing video records of ENF adhesive bonding specimens during the deformation process (Chai, 1992, 1993a). In all these figures, the numerical results seem to agree fairly well with the experiments.

A simplified shear-lag analysis, based on strength of material approximations for the adherend deformation, was recently developed for the specimens shown in Fig. 1 (Chai, 1992). The main simplifications concerning the adhesive layer in that analysis are: (a) the adhesive thickness is vanishingly small compared with the thickness of the adherends; (b) neglect of all the stress components in the interlayer but the shear stress; (c) neglect of the variations of shear stress across the bond; (d) elastic–perfectly plastic adhesive response. The shear-lag model predictions of the plastic zone characteristics also agreed well with

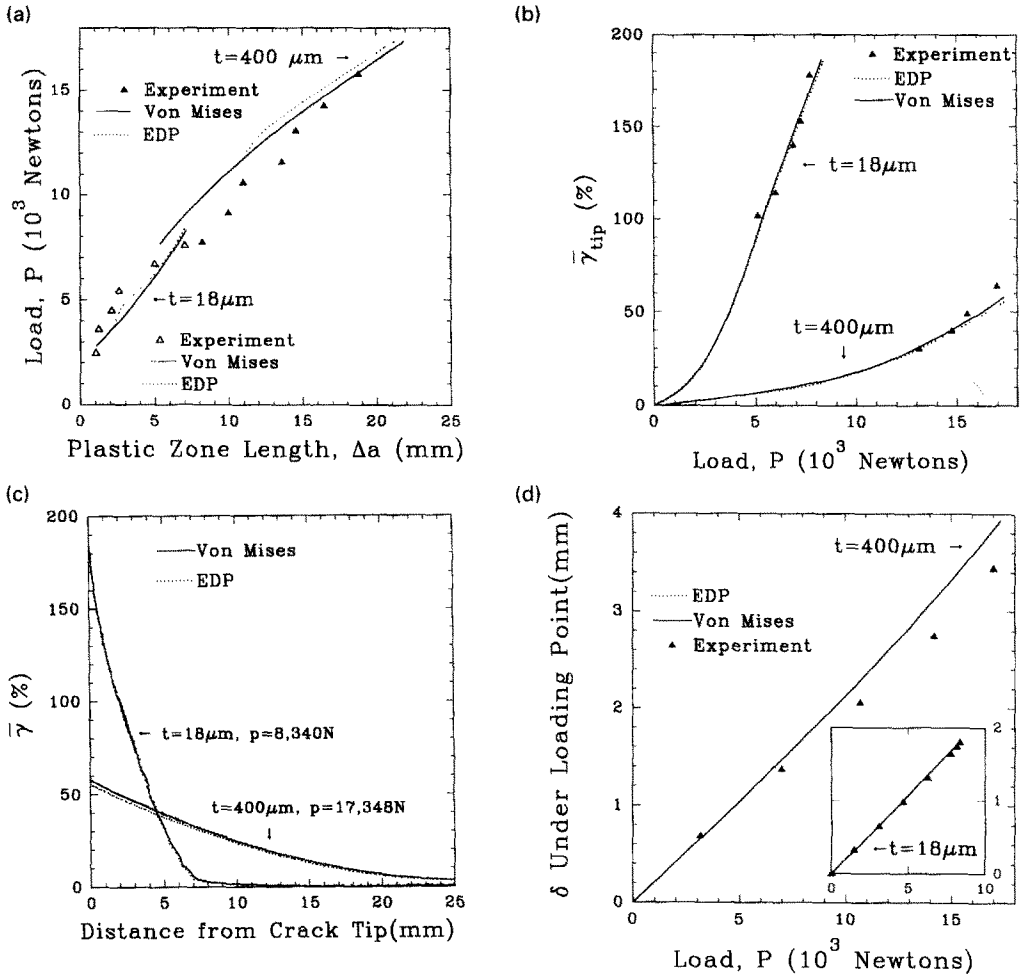

Fig. 5. The variation of the plastic zone at the crack tip with load (a), the variation of average shear strain at the crack tip with load (b), the distribution of average shear strain along the plastic zone for a given load (c), and the variation of the deflection under load with load (d), ENF specimen, J_2 flow and EDP flow with $\lambda = 1.4$ and $\psi = 0$. Adhesive material No. 1 ($t = 0.4$ mm) and No. 2 ($t = 18$ μm). For each plot, the experimental data shown (Chai, 1992, 1993a) correspond to the same specimen parameters as used in the finite element analysis.

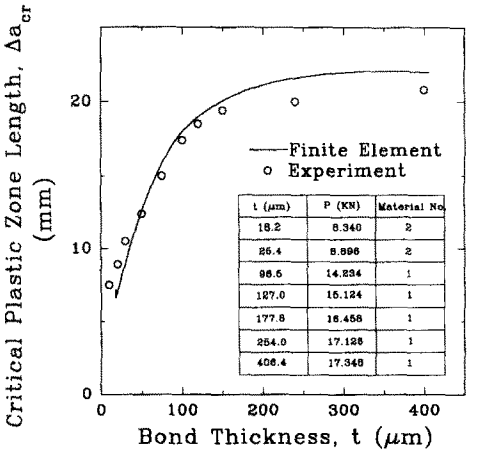

t (μm)	P (KN)	Material No.
18.2	8.340	2
25.4	8.896	2
96.5	14.234	1
127.0	15.124	1
177.8	16.456	1
254.0	17.128	1
406.4	17.348	1

Fig. 6. The variation of the critical plastic zone length with bond thickness, ENF specimen. Experimental data (open circles) (Chai, 1988) and finite element results (solid line) pertaining to J_2 material model. The insert specifies input parameters used in the finite element analysis.

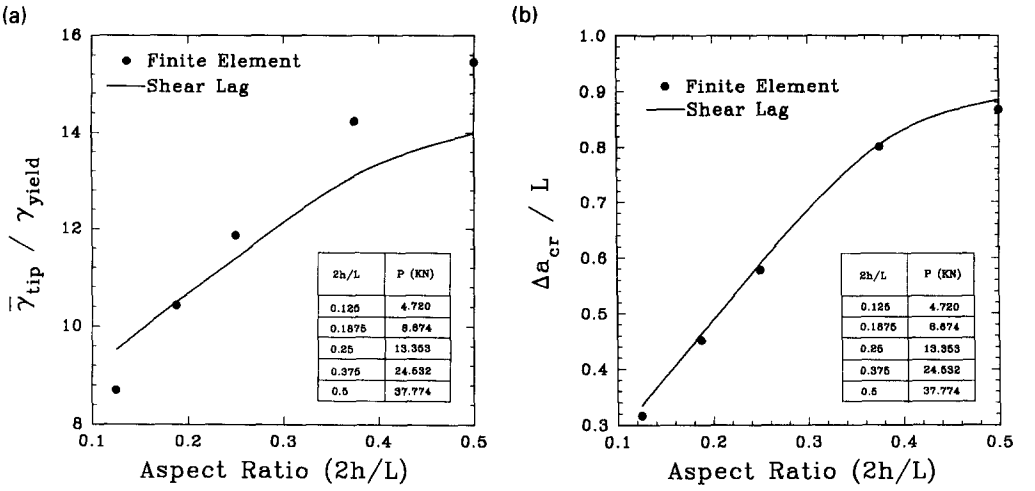

Fig. 7. The variation of normalized average shear strain at the crack tip (a) and of normalized critical plastic zone length (b) with beam slenderness ratio, $2h/L$. ELS specimen, with h set as a variable, $t = 0.4$ mm. Solid circles represent J_2 material model with adhesive material No. 1. The inserts specify the parameters used in the finite element analyses. The solid lines represent the shear-lag model prediction (Chai, 1992).

experimental results (Chai, 1992). This model, however, is incapable of reproducing the local behavior at the crack tip and even "global" responses (e.g. $\bar{\gamma}$ and Δa) if the specimen's arms are relatively thick.

The applicable range of the shear-lag model can be assessed from Fig. 7, which compares the shear-lag and the finite element predictions of the critical $\bar{\gamma}$ at the crack tip and the critical plastic zone length at various slenderness ratios ($2h/L$) of the split beams. The results in these figures pertain to the ELS specimen. Details of the specimen configurations used are listed in the figures. Figure 7(a) shows that the shear-lag model agrees well with the finite element results up to a slenderness ratio of approximately 0.25; for larger ratios the difference in the predictions increases gradually, reaching over 25% when $2h/L$ equals 0.5. One also observes from Fig. 7(a) that the shear-lag model noticeably departs from the finite element analysis when the slenderness ratio is decreased from approximately 0.15. This departure is most likely due to the effect of the relatively thick bond used (i.e. $t = 0.4$ mm), which is completely neglected in the shear-lag model (i.e. the model assumes that $t = 0$). In contrast to Fig. 7(a), Fig. 7(b) shows that the plastic zone length predicted by the shear-lag model agrees well with the finite element results for all slenderness ratios considered. This is clearly because the zone length is a less sensitive quantity than the shear strain. The applicability of the shear-lag model can also be assessed from Fig. 8, which shows the distance from the crack tip over which the shear strain first becomes uniform (to within a 10% variation across the bond), Δx, as a function of bond thickness. The specific bond configurations used are listed in the figure. The load in each case is the experimentally obtained critical load for crack propagation (Chai, 1988, 1992, 1993a). As shown, for $t > 0.1$ mm, the strain inhomogeneity seems to extend five to six bond thicknesses ahead of the tip. For thinner bonds, the span of strain inhomogeneity gradually declines, becoming of the order of one bond thickness in the micrometer thickness range.

The fracture behavior of adhesive bonds is greatly affected by the mechanical properties of the interlayer. For a brittle epoxy adhesive, the fracture process in mode II was found to start with the formation of tensile microcracks ahead of the crack tip and to end with the linkage of adjacent microcracks through growth along the interface (Chai, 1988, 1993a). In contrast, for a ductile adhesive, the crack grew from the tip (Chai, 1993a). Common to both adhesive systems, however, was the fact that for a given bond thickness, the critical average shear strain at the crack tip agreed fairly well with the ultimate shear strain of the unflawed adhesive interlayer (Chai, 1993a), the latter of which was determined using the napkin ring test specimen (Chai, 1993b). It should be noted that this correspondence held

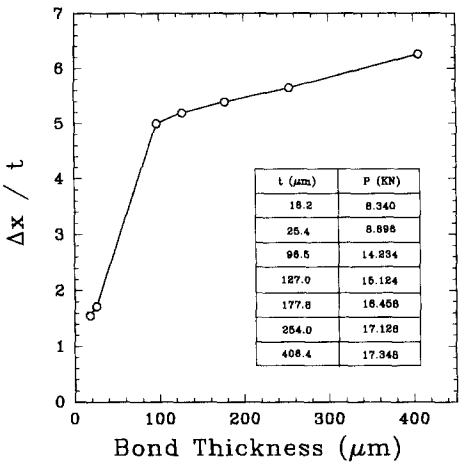

Fig. 8. The distance from the crack tip at which the adhesive shear strain begins to be uniform across the bond, Δx, as a function of bond thickness. ENF specimen, J_2 material model. The specimen parameters used to generate the individual finite element point are listed in the figure.

true only for relatively thin bonds. If one assumes that the shear strain in the napkin ring test is homogeneous across the bond, then the agreement noted above would seem at odds with the observation that the shear strain for the ductile BP-907 adhesive tended to localize at the crack tip (Chai, 1993a), and that this local strain which governs crack propagation may well exceed the average shear strain at the tip. A closer examination of the napkin ring test results shows, however, that the shear strain at the time of bond failure is not entirely uniform across the bond. As shown in Fig. 8 by Chai (1993b), final bond separation was the result of the coalescence of large voids that formed during the deformation process. It is also apparent from this figure that the magnitude of the local shear strain that developed around such voids considerably exceeds the average shear strain in the bond. Accordingly, the apparent discrepancy noted above can only be reconciled if one assumes that the degree of strain localization around such voids is similar to that developed at the tip of a large crack. Under this assumption, the average shear strain at the crack tip becomes a viable quantity for predicting crack propagation in the bond.

Another parameter that may affect fracture in ductile materials is the mean stress; large hydrostatic tension is known to cause failure through void growth and coalescence. Figure 4 shows that for both the thick and the thin bonds, the mean stress in the interlayer is negative (compression) and it declines monotonically with increasing distance from the crack tip. The maximum value in the case of the 18 μm thick bond is approximately the same as the uniaxial compression yield stress of the adhesive. This contrasts to the behavior for the analogous mode I loading case (Varias *et al.*, 1991) where the largest mean stress, occurring a few bond thicknesses ahead of the crack tip, may be several times the uniaxial yield stress in tension. Although the largest mean stress for the 18 μm thick bond is more than two fold larger than that for the 0.4 mm thick bond (see Fig. 4), the napkin ring tests show that only in the latter case did void growth and coalescence occurred (Chai, 1992b). This is possibly because in a thin interlayer the concentration of strains around voids is reduced due to interference with the relatively rigid adherends. More quantitative information on the void size–adhesive thickness interaction would be needed to understand the final fracture process in adhesive bonds better. Some work on this subject already exists in the literature (Tvergaard, 1991).

5. SUMMARY AND CONCLUSIONS

The distribution of elastoplastic stresses and strains in cracked adhesive bonds subjected to shear loading was determined from a large strain, quasi-static finite element analysis. The adhesive post-yield behavior was modeled by the J_2 criterion with associated

flow rule and by a modified Mohr–Coulomb criterion with non-associated flow rule. Isotropic strain hardening was considered for both material models.

A narrow region of intense plastic deformation dominated by shear was developed at the very edge of the crack tip. The shear strain within that region was several times the average shear strain at the crack tip. Increasing adhesive strain hardening or decreasing bond thickness tended to reduce strain localization; for a 0.4 mm and an 18 μm thick bond, the interlayer shear strain became homogeneous starting from approximately 2.4 mm and 25 μm ahead of the crack tip, respectively. The critical length of the plastic zone that developed ahead of the crack tip and the variation of average shear strain along that zone were little affected by the particular material model used. The variations with P of the plastic zone length and of the average shear strain at the crack tip agreed well with experimental results and also with a simplified shear-lag analysis, which neglects all adhesive stresses except the shear stress and disregards variations of this shear stress across the bond. The shear-lag analysis was found to predict quite accurately global mechanical responses as long as the slenderness ratio of the split beams is less than approximately 0.25. The mean stress in the interlayer was found to increase with decreasing bond thickness. Its maximum, which always occurred at the very edge of the crack tip, did not exceed the uniaxial yield stress for all bond thicknesses attempted.

Acknowledgements—We are grateful to Dr Gregory McKenna of the National Institute of Standards and Technology (NIST) for his helpful comments and discussions. We also extend our thanks to Dr Donald Hunston of NIST for the initiation of this collaboration.

REFERENCES

ABAQUS (1992). *Finite Element Analysis Code and Theory Manual*, Version 4.9. Hibbitt, Karlsson and Sorensen, RI, U.S.A.

Akisanya, A. R. and Fleck, N. F. (1992). Analysis of a wavy crack in sandwich specimens. *Int. J. Fract.* **55,** 29–45.

Anderson, G. P., Bennett, S. J. and DeVries, K. L. (1977). *Analysis and Testing of Adhesive Bonds.* Academic Press, New York.

Argon, A. S., Andrews, R. D., Godrick, J. A. and Whitney, W. (1968). Plastic deformation bands in glassy polystyrene. *J. Appl. Physics* **39,** 1899–1906.

Bauwens, J. C. (1970). Yield condition and propagation of Luders' lines in tension–torsion experiments on poly(vinyl chloride). *J. Polymer Sci. Part A-2* **8,** 893–901.

Bowden, P. B. and Jukes, J. A. (1972). The plastic flow of isotropic polymers. *J. Mater. Sci.* **7,** 52–63.

Brady, T. E. and Yeh, G. S. Y. (1971). Yielding behavior of glassy amorphous polymers. *J. Appl. Physics* **42,** 4622–4630.

Briscoe, B. J. and Tabor, D. (1978). Friction and wear of polymers: the role of mechanical properties. *British Polymer J.* **10,** 74–78.

Cao, H. C. and Evans, A. G. (1991). On crack extension in ductile/brittle laminates. *Acta Metall. Mater.* **39,** 2997–3005.

Chai, H. (1988). Shear fracture. *Int. J. Fract.* **37,** 137–159.

Chai, H. (1992). Micromechanics of shear deformations in cracked bonded joints. *Int. J. Fract.* **58,** 223–239.

Chai, H. (1993a). Observation of deformation and damage at the tip of cracks in adhesive bonds loaded in shear and assessment of a criterion for fracture. *Int. J. Fract.* **60,** 311–326.

Chai, H. (1993b). Deformation and failure of adhesive bonds under shear loading. *J. Mater. Sci.* **28,** 494–506.

Chatterjee, S. N. (1991). Analysis of test specimens for interlaminar mode II fracture toughness—Part 2: effect of adhesive layers and material nonlinearities. *J. Composite Mater.* **25,** 494–511.

Chen, W. F. and Han, D. J. (1988). *Plasticity for Structural Engineers.* Springer-Verlag, Berlin.

Hart-Smith, L. J. (1981). Stress analysis: a continuum mechanics approach. In *Development in Adhesives*—2, (Edited by A. J. Kinloch), pp. 1–44. Applied Science Publishers, London.

Hunston, D. L., Kinloch, A. J. and Wang, S. S. (1989). Micromechanics of fracture in structural adhesive bonds. *J. Adhesion* **28,** 103–114.

Hutchinson, J. W. and Suo, Z. (1991). Mixed mode cracking in layered materials. *Adv. Appl. Mech.* **29,** 63–191.

Liechti, K. M. and Freda, T. (1989). On the use of laminated beams for the determination of pure and mixed-mode fracture properties of structural adhesives. *J. Adhesion* **29,** 145–169.

Pae, K. D. and Bhateja, S. K. (1971). The effect of hydrostatic pressure on the mechanical behavior of polymers. *J. Macromol. Sci.* **C13** (I), 1–75.

Pampillo, C. A. and Davis, L. A. (1971). Volume change during deformation and pressure dependence of yield stress. *J. Appl. Physics* **42,** 4674–4679.

Rice, J. R. (1975). *Constitutive Equations in Plasticity* (Edited by A. S. Argon). MIT Press, Cambridge, MA, U.S.A.

Silling, S. A. (1988). Numerical studies of loss of ellipticity near singularities in an elastic material. *J. Elasticity* **19,** 213–239.

Suo, Z., Bao, G. and Fan, B. (1992). Delamination R-curve phenomena due to damage. *J. Mech. Physics Solids* **40,** 1–16.

Tirosh, J. (1973). The effect of plasticity and crack blunting on the stress distribution in orthotropic composite materials. *J. Appl. Mech.* **40,** 785–790.
Trantina, G. G. (1972). Combined mode crack extension in adhesive bonds. *J. Composite Mater.* **6,** 371–384.
Tvergaard, Y. (1991). Failure by ductile cavity growth at a metal ceramic interface. *Acta Metall. Mater.* **39,** 419–426.
Varias, A. G., Suo, Z. and Shih, C. F. (1991). Ductile failure of a constrained metal foil. *J. Mech. Physics Solids,* **39,** 963–986.
Wang, S. S. and Yau, J. F. (1982). Interface cracks in adhesively bounded lap-shear joints. *Int. J. Fract.* **19,** 295–309.
Wang, T. T., Zupko, H. M., Wyndon, L. A. and Matsuoka, S. (1982). Dimensional and volumetric changes in cylindrical rods of polymers subjected to twist moment. *Polymer* **23,** 1407–1409.

APPENDIX A

Utilizing well-known expressions for the second and third invariant of the deviatoric stress tensor, the parameters r and q in eqn (3) can be expressed as

$$r^3 = (2\sigma_1-\sigma_2-\sigma_3)(2\sigma_2-\sigma_3-\sigma_1)(2\sigma_3-\sigma_2-\sigma_1)/2 \tag{A1}$$

$$q = \frac{1}{\sqrt{2}}[(\sigma_1-\sigma_2)^2+(\sigma_2-\sigma_3)^2+(\sigma_3-\sigma_1)^2]^{1/2}. \tag{A2}$$

Substitution of the conditions for uniaxial tension ($\sigma_1 = \sigma_t^0$, $\sigma_2 = \sigma_3 = 0$) in eqns (A1), (A2), (3) and (6) leads to

$$\tan\beta = \frac{3\left(\lambda-\frac{1}{K}\right)}{\lambda+1}. \tag{A3}$$

The parameter ϕ can be related to λ using Fig. A1 (Chen and Han, 1988)

$$\phi = \tan^{-1}\frac{(\lambda-1)}{2\sqrt{\lambda}}. \tag{A4}$$

Matching the EDP with the Mohr–Coulomb model for a triaxial compression loading case, one finds (ABAQUS, 1992)

$$\tan\beta = \frac{6\sin\phi}{3-\sin\phi}. \tag{A5}$$

Using eqn (A4) in eqn (A5), one has

$$\tan\beta = \frac{3(\lambda-1)}{(\lambda+2)}. \tag{A6}$$

Comparing eqns (A3) and (A6), one gets

$$K = \frac{(\lambda+2)}{(2\lambda+1)}. \tag{A7}$$

Therefore, all the material constants in the EDP model can be specified by the two independent material constants σ_t^0 and λ.

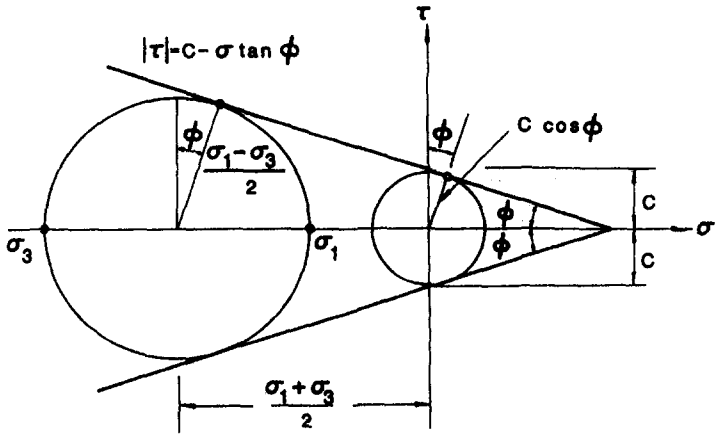

Fig. A1. Graphic representation of the Mohr–Coulomb yield condition (Chen and Han, 1988).